

# GALEX Absolute Calibration and Extinction Coefficients Based on White Dwarfs

Renae E. Wall<sup>1\*</sup>, Mukremin Kilic<sup>1</sup>, P. Bergeron<sup>2</sup>, B. Rolland<sup>2</sup>,  
C. Genest-Beaulieu<sup>2</sup>, A. Gianninas<sup>3</sup>

<sup>1</sup>Homer L. Dodge Department of Physics & Astronomy, University of Oklahoma, 440 W. Brooks St, Norman, OK 73019, USA

<sup>2</sup>Département de Physique, Université de Montréal, C. P. 6128, Succ. Centre-Ville, Montréal, QC H3C 3J7, Canada

<sup>3</sup>Department of Physics and Astronomy, Amherst College, 25 East Drive, Amherst, MA 01002

Submitted 9 September 2019

## ABSTRACT

We use 1837 DA white dwarfs with high signal to noise ratio spectra and Gaia parallaxes to verify the absolute calibration and extinction coefficients for the Galaxy Evolution Explorer (*GALEX*). We use white dwarfs within 100 pc to verify the linearity correction to the *GALEX* data. We find that the linearity correction is valid for magnitudes brighter than 15.95 and 16.95 for the Far Ultraviolet (FUV) and Near Ultraviolet (NUV) bands, respectively. We also use DA white dwarfs beyond 250 pc to calculate extinction coefficients in the FUV and NUV bands;  $R_{\text{FUV}} = 8.01 \pm 0.07$  and  $R_{\text{NUV}} = 6.72 \pm 0.04$ . These are consistent with the predicted extinction coefficients for Milky Way type dust in the FUV, but smaller than predictions in the NUV. With well understood optical spectra and state-of-the-art model atmosphere analysis, these white dwarfs currently provide the best constraints on the extinction coefficients for the *GALEX* data.

**Key words:** instrumentation: detectors — ultraviolet:general — telescopes — white dwarfs

## 1 INTRODUCTION

The *Galaxy Evolution Explorer* (*GALEX*) is the first space based mission to attempt an all-sky imaging survey in the ultraviolet (UV, [Martin et al. 2005](#)). In the ten years that it was operational, *GALEX* surveyed 26,000 square degrees of the sky as part of the All-sky Imaging Survey in two band passes: Far Ultraviolet (FUV) with a central wavelength of 1528 Å and Near Ultraviolet (NUV) with a central wavelength of 2271 Å ([Morrissey et al. 2005](#)). Although its primary goal was to study star formation and galaxy evolution, the first science goal was to determine UV calibration, particularly extinction ([Martin et al. 2005](#)).

There are two sources of nonlinearity in *GALEX* photometry: global nonlinearity due to the finite period required for the electronics to assemble photon lists and local nonlinearity near bright sources. [Morrissey et al. \(2007, see their Fig. 8\)](#) demonstrate that nonlinearity becomes significant ( $> 10\%$ ) above 109 and 311 counts  $\text{s}^{-1}$  in the FUV and NUV bands, respectively. These correspond to  $m_{\text{FUV}} \approx 14$  mag and  $m_{\text{NUV}} \approx 15$  mag. While the first nonlinearity is well understood, the second (local nonlinearity) complicates the standard star measurements.

*GALEX* observed 18 white dwarfs from the *Hubble Space Telescope* CALSPEC database ([Bohlin et al. 2001](#)) as standard stars. However, its photometric calibration relies primarily on the dimmest

star in this sample, LDS 749b, as all of the other standard stars observed are highly saturated. In fact, after [Bohlin & Koester \(2008\)](#) provided a better CALSPEC spectrum for LDS 749b, the *GALEX* magnitudes were shifted by  $\approx 0.04$  mag between the GR4/5 and GR6 data releases. Hence, it is important to verify the photometric calibration using fainter stars.

[Camarota & Holberg \(2014\)](#) verified the *GALEX* photometric calibration using 99 and 107 DA white dwarfs in the FUV and NUV, respectively, with magnitudes between 10 and 17.5 from the final GR7 *GALEX* data release. They found that a modest linearity correction is needed in this magnitude range. Although [Camarota & Holberg \(2014\)](#) postulate that their linearity correction should hold for stars as faint as 20th magnitude, they point out the need for a larger sample size and the characterization of extinction in the *GALEX* bands. In this work, we investigate the validity of the [Camarota & Holberg \(2014\)](#) linearity correction for a large sample of DA white dwarfs from the Sloan Digital Sky Survey (SDSS), particularly probing the fainter magnitudes.

There is a broad range of *GALEX* extinction coefficients reported in the literature. These coefficients are defined as

$$R_{\lambda} = \frac{A_{\lambda}}{E(B - V)}, \quad (1)$$

where  $A_{\lambda}$  is the total absorption along the line of sight to an object and  $E(B - V)$  is the reddening. [Bianchi \(2011\)](#) provided theoretical estimates of  $R_{\text{FUV}} = 8.06$  and  $R_{\text{NUV}} = 7.95$  for Milky Way type

\* rnenwall@ou.edu

dust and  $R_{\text{FUV}} = 12.68$  and  $R_{\text{NUV}} = 8.08$  for the Small Magellanic Cloud (SMC) type dust. [Yuan et al. \(2013\)](#) found empirical values of  $R_{\text{FUV}} = 4.37 - 4.89$  and  $R_{\text{NUV}} = 7.06 - 7.24$ . The latter authors used the ‘standard pair’ technique ([Stecher 1965](#)), where two stars of the same spectral type, one in an area with low extinction and one in an area of high extinction, are compared. Those stars with low extinction, the control sample, are used to determine the intrinsic colors of the corresponding stars with high extinction, the target sample. [Yuan et al. \(2013\)](#) examined a target sample of 1396 stars and a control sample of 16405 stars from the GALEX fifth data release. Most of these stars were classified as FGK dwarfs, with a small fraction of A dwarfs and KM giants. However, there is a great deal of scatter and uncertainty in their derivation of  $R_{\text{FUV}}$  and  $R_{\text{NUV}}$ , and [Yuan et al. \(2013\)](#) caution against using their GALEX extinction coefficients. In this work, we re-derive the GALEX extinction coefficients using a large sample of DA white dwarf stars with high S/N SDSS spectra and Gaia parallaxes to obtain a more reliable estimate.

We present the white dwarf sample used in this study in Section 2 and describe our calculation of the synthetic magnitudes in Section 3. Our analysis of nonlinearity is presented in Section 4 followed by our derivation of the GALEX extinction coefficients in Section 5. The  $3\sigma$  outliers are discussed in Section 6, and we conclude in Section 7.

## 2 SAMPLE SELECTION

In order to improve calibrations for the GALEX data, we select all spectroscopically confirmed DA white dwarfs from the SDSS data releases 7, 10, and 12 with  $S/N \geq 20$  spectra ([Kleinman et al. 2013](#); [Kepler et al. 2015, 2016](#)). This selection insures that the  $T_{\text{eff}}$  and  $\log g$  measurements are precise enough to model the emergent stellar fluxes in the UV bands. We focus on DA white dwarfs due to our good understanding of their opacities and atmospheres ([Holberg & Bergeron 2006](#)). We cross reference our initial sample of 3733 DA white dwarfs from the SDSS with Pan-STARRS, and we cross reference our sample once more with *Gaia* DR2, selecting all stars with  $\text{parallax/error} \geq 5$ . We then cross reference our sample with the GALEX catalog of unique UV sources from the All Sky Imaging Survey (GUVcat) presented in [Bianchi et al. \(2017\)](#). We use a search radius of  $2''$  and find a total of 1837 stars with GALEX photometry.

We break our initial sample of stars into two groups based on *Gaia* distance: stars within 100 pc and stars further than 250 pc. There are 339 (627) and 451 (628) stars with FUV and NUV photometry in the 100 ( $d > 250$ ) pc sample, respectively. We leave the examination of stars between 100 and 250 pc for future work. The local interstellar medium is relatively devoid of cold neutral gas, up to about 100 pc, the boundary of the Local Bubble ([Lallement et al. 2003](#); [Redfield 2006](#)). Since extinction is not an issue for the 100 pc sample, we use it to verify the GALEX photometric calibration. The  $d > 250$  pc sample suffers from full extinction, and we use it to calculate the extinction coefficients in both the FUV and NUV bands.

## 3 SYNTHETIC MAGNITUDES

[Genest-Beaulieu & Bergeron \(2019\)](#) found a systematic offset between temperatures derived using the spectroscopic ([Bergeron et al. 1992](#)) and photometric ([Bergeron et al. 1997](#)) techniques. They determine that this offset is caused by inaccuracies in the treatment of

Stark broadening in their model spectra. The photometric technique is less sensitive to the input physics of the models, so we adopted it for this work. We use SDSS *u* and Pan-STARRS grizy photometry and *Gaia* parallaxes to derive photometric temperatures and radii for all stars in our final sample. These temperature and radius measurements are then used to calculate a model spectrum for each white dwarf in the 100 pc sample.

To estimate the average flux in a given bandpass,  $f_{\lambda}^m$ , we use the equation

$$f_{\lambda}^m = \frac{\int_0^{\infty} f_{\lambda} S_m(\lambda) \lambda d\lambda}{\int_0^{\infty} S_m(\lambda) \lambda d\lambda}, \quad (2)$$

where  $S_m(\lambda)$  is the transmission function of the corresponding bandpass, and  $f_{\lambda}$  is the monochromatic flux from the star received at Earth ([Bergeron et al. 1997](#); [Gianninas et al. 2011](#)). SDSS, Pan-STARRS, and GALEX use the AB magnitude system. We transform the average flux in a given bandpass to an average magnitude using the equation

$$m = -2.5 \log f_{\nu}^m - 48.6. \quad (3)$$

This procedure enables us to calculate the absolute magnitude of each star in each filter. We use the observed and dereddened SDSS magnitudes for the  $d < 100$  and  $d > 250$  pc samples, respectively.

## 4 GALEX PHOTOMETRIC CALIBRATION

Our 100 pc SDSS sample contains few stars brighter than 14th magnitude. In order to constrain the fit for both faint and bright white dwarfs, we extend our sample to include the 100 pc white dwarfs from [Camarota & Holberg \(2014\)](#) and [Gianninas et al. \(2011\)](#). Figure 1 compares the observed and predicted synthetic magnitudes for this sample in both bands. The solid and dashed lines show a quadratic polynomial fit to the data and the one-to-one line, respectively. Stars with  $T_{\text{eff}}$  below 11,000 K are represented by yellow triangles. Stars below this temperature suffer from the red wing of the Ly $\alpha$  opacity, which affects the ultraviolet more strongly than the optical ([Kowalski & Saumon 2006](#)). The  $3\sigma$  outliers that are known double degenerates, white dwarf + main sequence binaries, and ZZ Ceti are marked by cyan triangles, green diamonds, and magenta pentagons, respectively. Previously unknown  $3\sigma$  outliers in our polynomial fit are plotted as red squares. All  $3\sigma$  outliers are excluded from this fit. We further discuss these outliers in Section 6.

Our quadratic fits are represented by the expression

$$m_{\text{obs}} = c_2 m_{\text{synth}}^2 + c_1 m_{\text{synth}} + c_0, \quad (4)$$

where  $m_{\text{obs}}$  and  $m_{\text{synth}}$  are the observed and synthetic GALEX magnitudes, respectively. The best fit values of the fitting coefficients  $c_0$ ,  $c_1$ , and  $c_2$  are given in Table 2.

[Camarota & Holberg \(2014\)](#) found a non-linear correlation and small offset between GALEX fluxes and predicted fluxes for their sample. Their quadratic fit is shown as a dotted line in Figure 1 and is based on about 100 DA white dwarfs with FUV and NUV magnitudes between 10 and 17.5 mag. However, they only have 6-8 stars fainter than 17th magnitude in their sample, hence the fit is relatively unconstrained at the faint end. The dotted line significantly underpredicts the observed magnitudes in both FUV and NUV bands, and is clearly not useful below 17th magnitude.

**Table 1.** Properties of stars within 100 pc in our sample. Stars with WD names are from [Gianninas et al. \(2011\)](#). The full table is available online.

Star	Synthetic FUV mag	Synthetic NUV mag	Observed FUV mag	Observed NUV mag
J000410.42-034008.60	25.802	19.201	...	19.142 ± 0.070
J001339.11+001924.90	19.769	16.403	19.756 ± 0.103	16.449 ± 0.014
J002049.39+004435.10	22.29	17.96	22.194 ± 0.369	17.937 ± 0.027
WD0023-109	20.714	17.385	19.394 ± 0.093	17.203 ± 0.019
J002634.39+353337.60	23.59	19.187	...	19.132 ± 0.072
J003328.03+054039.18	26.94	20.354	...	20.167 ± 0.142
J003511.63+001150.40	20.592	17.417	20.817 ± 0.151	17.511 ± 0.022
WD0033+016	18.921	16.312	18.727 ± 0.077	16.368 ± 0.016
WD0037-006	16.92	15.548	15.456 ± 0.016	15.299 ± 0.010
J004511.19+090445.37	25.926	19.923	...	19.922 ± 0.128
WD0048+202	14.519	14.839	14.565 ± 0.008	14.837 ± 0.005
J005438.84-095219.70	22.299	18.077	22.158 ± 0.497	17.942 ± 0.043
WD0058-044	14.933	15.139	14.934 ± 0.016	15.182 ± 0.011
WD0100-036	22.062	17.91	21.635 ± 0.369	17.885 ± 0.039
WD0101+059	16.318	16.138	16.219 ± 0.021	16.132 ± 0.012
WD0101+048	20.513	15.622	19.545 ± 0.103	15.528 ± 0.011
WD0102+095	13.163	13.626	13.130 ± 0.007	13.801 ± 0.006
J010543.14-092054.60	24.111	18.849	...	18.729 ± 0.046
WD0104+015	23.286	18.723	21.735 ± 0.448	18.408 ± 0.063
WD0107+267	15.156	15.181	15.144 ± 0.008	15.231 ± 0.005

**Table 2.** Fitting parameters for the linearity correction in the FUV and NUV bands (see Eq 4.)

Property	FUV	NUV
$c_0$	13.23	10.49
$c_1$	-0.727	-0.31
$c_2$	0.057	0.041
Range	≤ 15.95 mag	≤ 16.95 mag

**Table 3.** Inverse quadratic corrections for the FUV and NUV bands (see Eq 5.)

Property	FUV	NUV
$c_0$	6.412	3.778
$c_1$	17.63	24.337
$c_2$	-192.135	-241.018

With a significantly larger number of fainter DA white dwarfs, we are able to test for non-linearities in the data down to magnitudes fainter than 20. We note that stars with  $T_{\text{eff}}$  below 11,000 K have systematically fainter synthetic magnitudes in the FUV, while there is no systematic offset in the NUV. Since these stars are affected by the red wing of the Ly $\alpha$  opacity ([Kowalski & Saumon 2006](#)), our results indicate that this opacity source is well handled in our models for the NUV, while the modeling of this opacity should be revisited for the FUV. To remove this systematic effect from our fit, we first fit the full sample to calculate the magnitude where the full quadratic fit crosses the one-to-one line for the FUV and NUV. Only stars brighter than these magnitudes, 15.95 mag (FUV) and 16.95 mag (NUV), will require a linearity correction. To determine the linearity correction, we then fit only stars brighter than 15.95 mag (FUV) and 16.95 mag (NUV). This is our final quadratic fit which is plotted in Figure 1. Our linearity corrections are not statistically different from those presented in [Camarota & Holberg \(2014\)](#). To convert the observed *GALEX* magnitudes into corrected magnitudes, we find the quadratic solutions to the linearity corrections shown in Figure 1. Our final corrections take the form

$$m_{\text{corr}} = c_0 + (c_1 m_{\text{obs}} + c_2)^{1/2}, \tag{5}$$

where  $m_{\text{obs}}$  and  $m_{\text{corr}}$  are the observed and corrected *GALEX* magnitudes, respectively. The calculated constants  $c_0$ ,  $c_1$ , and  $c_2$  are given in Table 3. These corrections are applicable to objects brighter than 15.95 mag and 16.95 mag in the FUV and NUV, respectively.

## 5 EXTINCTION COEFFICIENTS

After revisiting the linearity corrections and determining the magnitudes they are valid over, we examine the sample of SDSS DA white dwarfs with Gaia distances beyond 250 pc. We apply the linearity corrections given in Table 3 only to those stars brighter than our cut-off magnitudes. Figure 2 shows the observed versus synthetic magnitudes for the 250 pc white dwarf sample. These stars experience full extinction, which leads to observed FUV and NUV photometry fainter than expected.

We calculate the  $R$  value in the NUV and FUV bands for each star using Equation 1, the total absorption in each filter  $A_\lambda$  (the difference between the synthetic and observed magnitude), and  $E(B - V)$  from [Schlafly & Finkbeiner \(2011\)](#). We find 9 stars in the FUV and 18 stars in the NUV with negative  $R$  values. These stars, as well as the  $4\sigma$  outliers, are excluded from the weighted average of the  $R$  values.

Figure 3 shows the distribution of the  $R$  values in the FUV and NUV filters. Since the  $R$  values for some stars have relatively large uncertainties, here we plot weighted histograms, where each  $R$  value only contributes its associated error towards the bin count (instead of 1). This figure reveals a relatively large spread in  $R$  for both filters, with a standard deviation  $\sim 3$ . This spread in  $R$  values indicates that we cannot characterize the interstellar extinction by a universal reddening law for all lines of sight within the SDSS footprint. However, our best estimate, the weighted mean values, are  $R_{\text{FUV}} = 8.01 \pm 0.07$  and  $R_{\text{NUV}} = 6.79 \pm 0.04$ .

[Bianchi \(2011\)](#) estimated *GALEX* extinction coefficients using progressively reddened models for stars with  $T_{\text{eff}} = 15,000 - 30,000$

**Table 4.** Properties of stars beyond 250 pc in our sample. Stars with WD names are from [Gianninas et al. \(2011\)](#). The full table is available online.

Star	Synthetic FUV mag	Synthetic NUV mag	Observed FUV mag	Observed NUV mag
J000302.59+240555.80	18.699	18.73	19.461 ± 0.077	19.241 ± 0.039
J000626.69+242441.70	18.196	18.372	18.964 ± 0.067	18.995 ± 0.031
J001043.55+253829.18	15.968	16.526	16.395 ± 0.020	16.890 ± 0.010
J001549.44+245604.91	15.691	16.253	16.038 ± 0.016	16.558 ± 0.009
J001712.70+250443.04	17.95	18.125	18.218 ± 0.047	18.391 ± 0.026
J002126.69-093714.20	17.688	17.946	18.049 ± 0.035	18.252 ± 0.024
WD0019+150	15.3	15.863	15.697 ± 0.018	16.160 ± 0.013
J002636.48-100330.50	17.116	17.444	17.552 ± 0.050	17.757 ± 0.024
J002806.49+010112.20	16.185	16.67	16.477 ± 0.028	16.885 ± 0.022
J003533.74+240253.17	17.293	17.688	17.683 ± 0.057	18.139 ± 0.048
J004346.36+254910.50	18.482	18.482	18.695 ± 0.120	18.647 ± 0.065
J004648.66+250915.10	17.924	18.095	18.405 ± 0.091	18.525 ± 0.043
J005547.78-084507.30	13.795	14.376	14.885 ± 0.014	15.160 ± 0.011
J010810.17+183120.46	16.957	17.351	17.586 ± 0.065	17.956 ± 0.044
J011100.64+001807.20	19.873	19.182	20.996 ± 0.320	19.425 ± 0.109
J011428.32+215310.79	16.21	16.764	16.439 ± 0.034	17.012 ± 0.027
J011541.62+310404.20	16.432	16.952	16.963 ± 0.042	17.318 ± 0.030
J012041.19+395307.20	17.423	17.683	17.671 ± 0.067	17.923 ± 0.033
J012318.14+330014.34	17.713	17.892	17.927 ± 0.043	18.12 ± 0.029
J012601.53+332523.49	16.21	16.702	16.917 ± 0.042	17.252 ± 0.022

K. Since *GALEX* NUV band includes the strong broad absorption feature at 2175 Å, they predict an overall absorption that is similar in both the FUV and NUV bands. For Milky Way type dust, they predict  $R_{\text{FUV}} \approx R_{\text{NUV}} \approx 8.0$ . However, for UV-steep extinction curves like those of the Large Magellanic Cloud (LMC) and the SMC, the increase in absorption is larger in the FUV and the 2175 Å bump is less pronounced, resulting in estimates of  $R_{\text{FUV}} = 8.6\text{--}12.7$  and  $R_{\text{NUV}} = 7.0\text{--}8.1$ . Hence, some of the scatter seen in Figure 3 can be explained by the differences in extinction curves along different line of sights as sampled by our targets.

Empirical constraints on *GALEX* extinction by [Yuan et al. \(2013\)](#) agree relatively well in the NUV but they differ significantly in the FUV. [Yuan et al. \(2013\)](#) measure  $R_{\text{NUV}} = 7.24 \pm 0.08$  or  $7.06 \pm 0.22$  and  $R_{\text{FUV}} = 4.89 \pm 0.60$  or  $4.37 \pm 0.54$ . Our FUV extinction coefficient is significantly larger than the [Yuan et al. \(2013\)](#) estimate and in good agreement with the [Bianchi \(2011\)](#) estimate. Given the simplicity of DA white dwarf photospheres, white dwarfs are excellent spectrophotometric standard stars and our empirical results are significantly more precise than previous FUV and NUV extinction coefficient measurements.

Figure 4 shows a comparison between the observed FUV/NUV magnitudes corrected for non-linearity and extinction and synthetic magnitudes for the  $d > 250$  pc sample using our best-estimates of  $R_{\text{FUV}} = 8.01 \pm 0.07$  and  $R_{\text{NUV}} = 6.79 \pm 0.04$ . These R values provide excellent corrections for our dataset, as the majority of the objects fall on or near the one-to-one line (shown as a blue dashed line). The red squares mark the  $4\sigma$  outliers from the one-to-one line. The yellow square marks J211607.27+004503.17, a previously known candidate binary system ([Baxter et al. 2014](#)). We further discuss the unknown outliers in Section 6.

## 6 OUTLIERS

Here we revisit the 3 and  $4\sigma$  outliers identified in the 100 and 250 pc samples in Sections 4 and 5, respectively. One possible cause of a significant difference between the observed and model FUV and NUV magnitudes is the presence of an unseen companion. If

two stars are sufficiently close together to be unresolved in both *GALEX* and the SDSS observations, one could still identify the binary nature of the system through UV-excess, like the double white dwarf SDSS J125733.63+542850.5 ([Badenes et al. 2009](#); [Kulkarni & van Kerkwijk 2010](#); [Marsh et al. 2011](#); [Bours et al. 2015](#)). Note that this method only works for systems where there is a significant temperature difference between the two white dwarfs.

Out of our twelve total outliers, seven are previously known systems. Although WD0901+140 is a visual binary ([Farihi et al. 2005](#)), it was not resolved in *GALEX*. Of the five remaining outliers, the photometry of WD0846+335 is likely contaminated by a nearby background galaxy. In Figure 5, we plot the SEDs of the remaining four outliers. We plotted the SDSS and GUVcat fluxes as blue errorbars. Each of these objects has UV observations from other *GALEX* surveys. These fluxes are represented by the red errorbars. Model fluxes are represented by blue dots. J083029.77+085014.20 is sufficiently near to a bright star that its photometry was contaminated in the shallow AIS survey. Deeper surveys removed this contamination, as can be seen in Figure 5. J212411.99-072648.70 has a spectroscopic  $T_{\text{eff}}$  of 76,364 K from [Kleinman et al. \(2013\)](#), well above 35,000 K, the  $T_{\text{eff}}$  above which the photometric technique becomes less reliable ([Genest-Beaulieu & Bergeron 2019](#)). It is likely that the photometric  $T_{\text{eff}}$  is off, leading to the apparent UV excess. J060255.98+632304.80 has a  $T_{\text{eff}}$  of 11,078 K and a  $\log g$  of 7.7, placing this star within the ZZ Ceti instability strip (10,500-13,000K  $T_{\text{eff}}$ ). The UV excess is greater in other *GALEX* surveys. ZZ Ceti pulsations are stronger in the UV, so the UV excess could be due to pulsations as with WD1258+013. Further observations are needed to confirm that J060255.98+632304.80 is a ZZ Ceti. There are no obvious explanations for the UV excess of J091145.12+353135.60. Follow-up UV spectroscopy or radial velocity observations would be helpful in understanding the nature of this object.

## 7 CONCLUSIONS

We examine a sample of 1837 DA white dwarfs that were observed by both SDSS and *GALEX*. By combining our SDSS sample within

**Table 5.** Previously known binary or variable white dwarfs that are identified as outliers in this work.

Object	Type	Source
WD0037-006	Double-lined double degenerate	Koester et al. (2009)
WD0232+035	DA+dM	Kawka et al. (2008)
WD0901+140	Visual double degenerate	Farihi et al. (2005)
WD1019+462	WD+dM	Reid (1996)
WD1022+050	Double degenerate	Bragaglia et al. (1995)
WD1258+013	ZZ Ceti	Bergeron et al. (2004)
J211607.27+004503.17	Double degenerate candidate	Baxter et al. (2014)

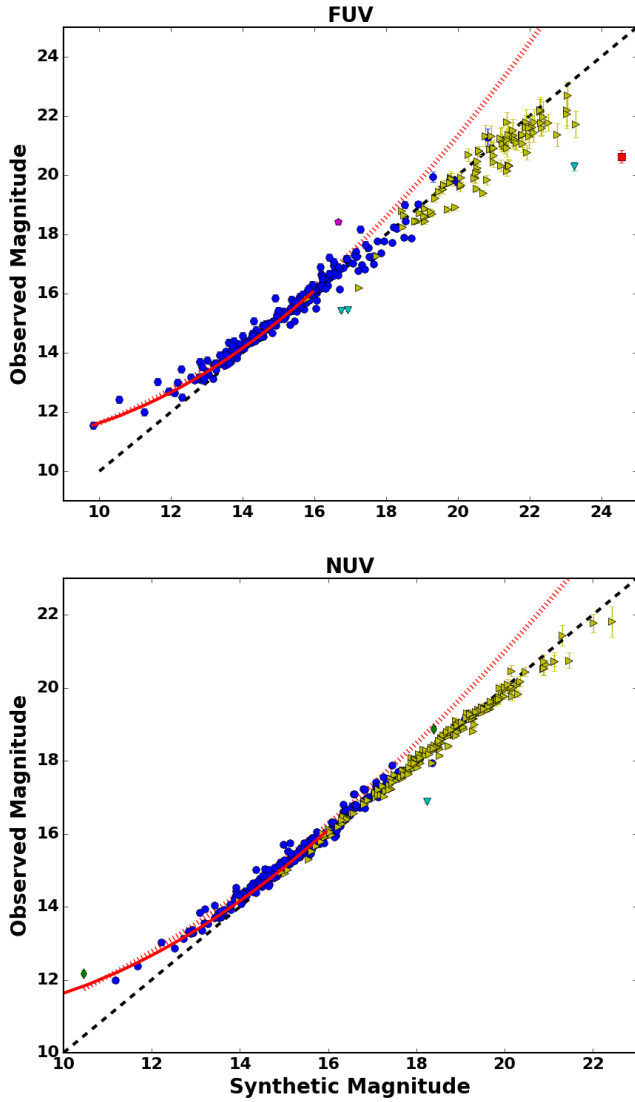


**Figure 1.** The linearity fit for stars within 100 pc in the FUV band (top) and the NUV band (bottom). The quadratic linearity fit from Camarota & Holberg (2014) is marked as the red dashed line. Our linearity fit is plotted in solid red. The black dashed line is the one-to-one correlation. Stars with  $T_{\text{eff}}$  below 11,000 K are plotted as yellow triangles. Cyan triangles are known double degenerate systems and green diamonds are previously known WD+main sequence binaries. The magenta pentagon marks the ZZ Ceti WD1258+013. Previously unknown  $3\sigma$  outliers are plotted as red squares.

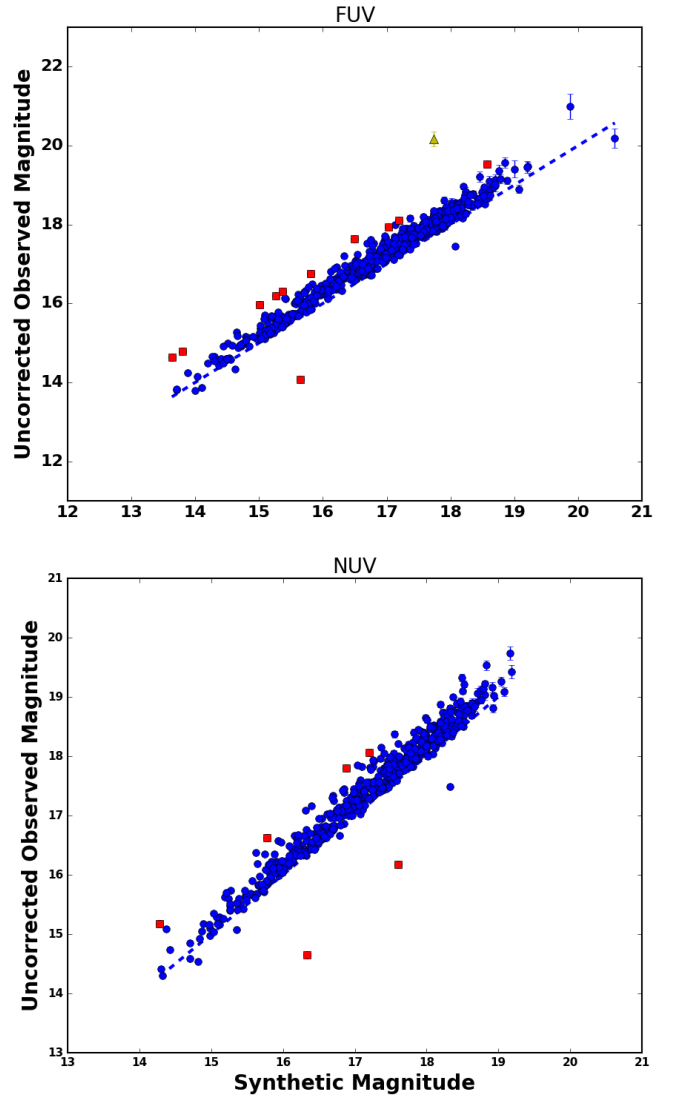


**Figure 2.** Uncorrected versus model magnitudes for stars beyond 250 pc in the FUV and NUV bands. The blue dashed line is the one-to-one correlation and  $4\sigma$  outliers are plotted as red squares. The candidate double degenerate J211607.27+004503.17 is plotted as a yellow triangle.

100 pc and the bright white dwarf samples from Camarota & Holberg (2014) and Gianninas et al. (2011), we determine an improved linearity correction to the GALEX data. We determine that our linearity corrections are only necessary for objects brighter than 15.95 mag and 16.95 mag for the FUV and NUV bands, respec-

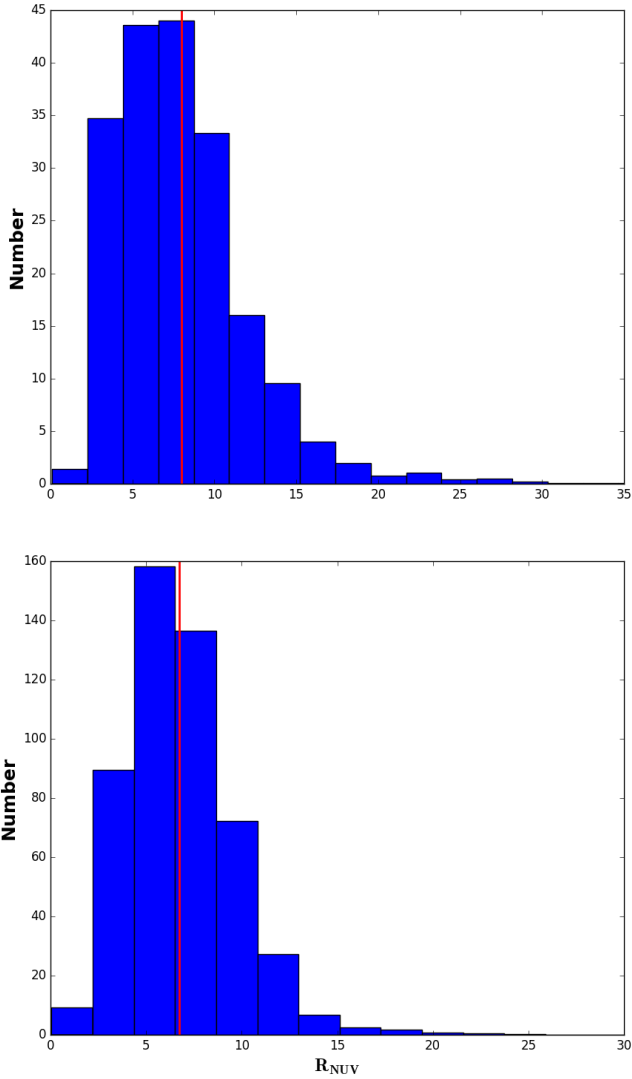


**Figure 3.** Histograms of weighted  $R$  values for FUV and NUV bands. The solid red line is the weighted average.

tively. We present new extinction coefficients for the *GALEX* bands:  $R_{\text{FUV}} = 8.01 \pm 0.07$  and  $R_{\text{NUV}} = 6.79 \pm 0.04$ . These white dwarfs currently provide the best constraints on the linearity corrections and extinction coefficients for *GALEX* data.

Here we present one application of our newly derived  $R$  values for identifying unusual white dwarfs. We identify seven previously known objects: three double degenerates (WD0037-006, WD0901+140, and WD1022+050), two white dwarf+main sequence binaries (WD1019+462 and WD0232+035), one ZZ Ceti (WD1258+013), and one double degenerate candidate (J211607.27+004503.17) as outliers. We find one previously unknown  $3\sigma$  outlier and four previously unknown  $4\sigma$  outliers. The UV-excesses of three of these objects (WD0846+335, J083029.77+085017.20, and J212411.99-072648.70) can be explained by contaminating background sources or inaccurate photometric solutions. Two outliers, J091145.12+353135.60 and J060255.98+632304.80, require follow-up spectroscopy to verify their natures. In the future, we will use our linearity corrections and

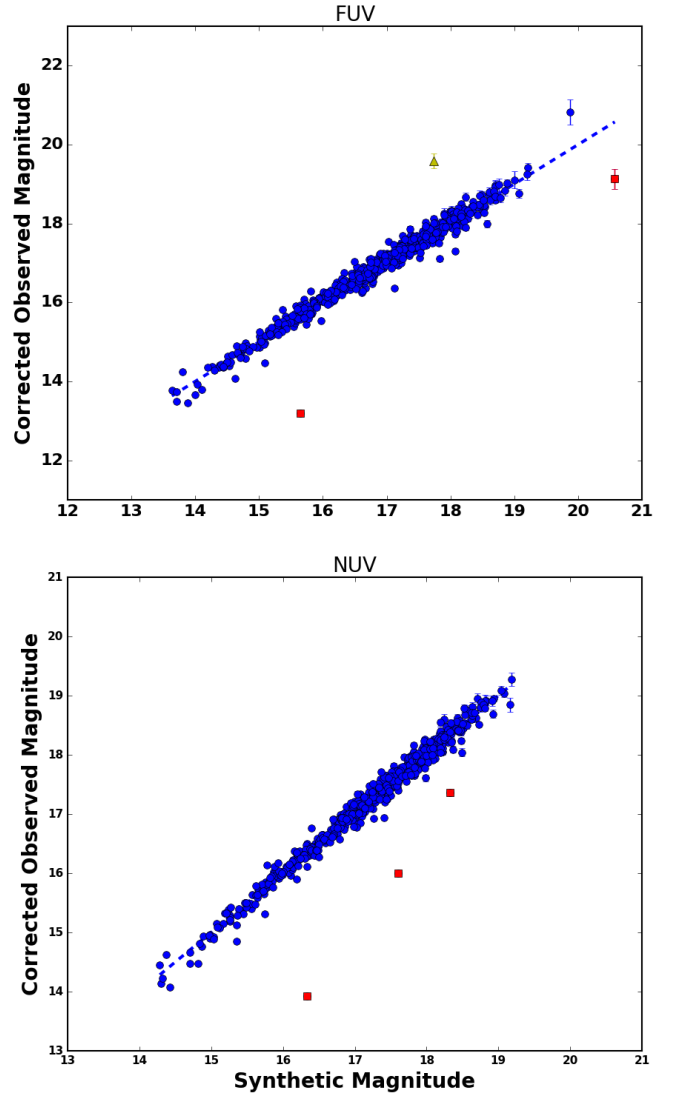


**Figure 4.** Extinction corrected versus model magnitudes for stars beyond 250 pc in the FUV and NUV bands. The blue dashed line is the one-to-one correlation and  $4\sigma$  outliers are plotted as red squares. The candidate double degenerate J211607.27+004503.17 is plotted as a yellow triangle.

our newly derived extinction coefficients to study the remainder of our SDSS sample and identify unusual objects.

#### ACKNOWLEDGEMENTS

This work is supported by the NASA Astrophysical Data Analysis Program grant NNX14AF65G. This work is supported in part by the NSERC Canada and by the Fund FRQ-NT (Québec). This work has made use of data from the European Space Agency (ESA) mission *Gaia* (<https://www.cosmos.esa.int/gaia>), processed by the *Gaia* Data Processing and Analysis Consortium (DPAC, <https://www.cosmos.esa.int/web/gaia/dpac/consortium>). Funding for the DPAC has been provided by national institutions, in particular the institutions participating in the *Gaia* Multilateral Agreement. We thank our referee, Jay Holberg, for his useful suggestions.

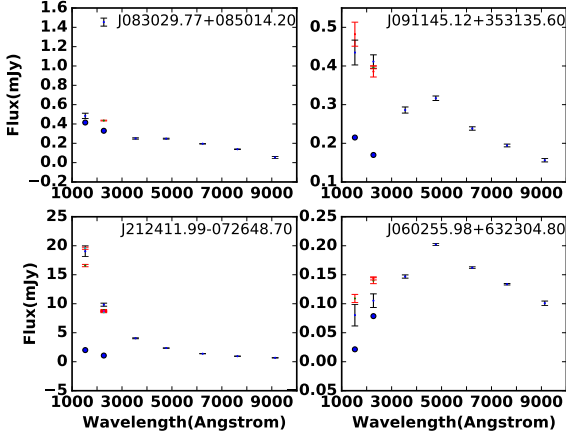


**Figure 5.** SEDs of four newly identified candidate UV-excess white dwarfs. Black errorbars represent fluxes from SDSS and GUVcat. Red errorbars represent fluxes from all other GALEX observations. Blue dots represent model fluxes. Note that two of these outliers, J0830+0850 and J2124-0726, likely have contaminated photometry or inaccurate photometric solutions.

## REFERENCES

- Badenes, C., Mullally, F., Thompson, S. E., et al. 2009, *ApJ*, 707, 971  
 Baxter, R. B., Dobbie, P. D., Parker, Q. A., et al., 2014, *MNRAS*, 440, 3184  
 Bergeron, P., Fontaine, G., Billères, M., Boudreault, S., & Green, E. M. 2004, *ApJ*, 600, 404  
 Bergeron, P., Leggett, S. K., & Ruiz, M. T. 2001, *ApJS*, 133, 413  
 Bergeron, P., Ruiz, M. T., & Leggett, S. K. 1997, *ApJS*, 108, 339  
 Bergeron, P., Saffer, R. A., & Liebert, J. 1992, *ApJ*, 394, 228.  
 Bergeron, P., Saumon, D., & Wesemael, F. 1995, *ApJ*, 443, 764  
 Bergeron, P., Wesemael, F., Lamontagne, R., et al. 1995, *ApJ*, 449, 258.  
 Bianchi, L. 2011, *Ap&SS*, 335, 51  
 Bianchi, L., Shiao, B., & Thilker, D. 2017, *ApJS*, 230, 24  
 Bohlin, R. C., Dickinson, M. E., & Calzetti, D. 2001, *AJ*, 122, 2118  
 Bohlin, R. C., & Koester, D. 2008, *AJ*, 135, 1092  
 Bours, M. C. P., Marsh, T. R., Gänsicke, B. T., et al. 2015, *MNRAS*, 450, 3966  
 Bragaglia, A., Renzini, A., & Bergeron, P. 1995, *ApJ*, 443, 735  
 Brown, W. R., Kilic, M., & Gianninas, A. 2017, *ApJ*, 839, 23  
 Camarota, L., & Holberg, J. B. 2014, *MNRAS*, 438, 3111  
 Farihi, J., Becklin, E. E., & Zuckerman, B. 2005, *ApJS*, 161, 394  
 Foreman-Mackey, D., Hogg, D. W., Lang, D., & Goodman, J. 2013, *PASP*, 125, 306  
 Gaia Collaboration, Babusiaux, C., van Leeuwen, F., et al. 2018, arXiv:1804.09378  
 Genest-Beaulieu, C., & Bergeron, P. 2019, *ApJ*, 871, 169.  
 Gianninas, A., Bergeron, P., & Ruiz, M. T. 2011, *ApJ*, 743, 138  
 Holberg, J. B., & Bergeron, P. 2006, *AJ*, 132, 1221  
 Kawka, A., Vennes, S., Dupuis, J., Chayer, P., & Lanz, T. 2008, *ApJ*, 675, 1518  
 Kepler, S. O., Pelisoli, I., Koester, D., et al. 2015, *MNRAS*, 446, 4078  
 Kepler, S. O., Pelisoli, I., Koester, D., et al. 2016, *MNRAS*, 455, 3413  
 Kleinman, S. J., Kepler, S. O., Koester, D., et al. 2013, *ApJS*, 204, 5  
 Koester, D., Voss, B., Napiwotzki, R., et al. 2009, *A&A*, 505, 441  
 Kowalski, P. M., & Saumon, D. 2006, *ApJ*, 651, L137.  
 Kulkarni, S. R., & van Kerkwijk, M. H. 2010, *ApJ*, 719, 1123.  
 Lallement, R., Welsh, B. Y., Vergely, J. L., Crifo, F., & Sfeir, D. 2003, *A&A*, 411, 447  
 Martin, D. C., Fanson, J., Schiminovich, D., et al. 2005, *ApJ*, 619, L1  
 Marsh, T. R., Gänsicke, B. T., Steeghs, D., et al. 2011, *ApJ*, 736, 95.  
 Morrissey, P., Schiminovich, D., Barlow, T. A., et al. 2005, *ApJ*, 619, L7  
 Morrissey, P., Conrow, T., Barlow, T. A., et al. 2007, *ApJS*, 173, 682

Redfield, S. 2006, *New Horizons in Astronomy: Frank N. Bash Symposium*, 352, 79

Reid, I. N. 1996, *AJ*, 111, 2000

Schlafly, E. F., & Finkbeiner, D. P. 2011, *ApJ*, 737, 103

Stecher, T. P. 1965, *ApJ*, 142, 1683

Yuan, H. B., Liu, X. W., & Xiang, M. S. 2013, *MNRAS*, 430, 2188

This paper has been typeset from a  $\text{\TeX}/\text{\LaTeX}$  file prepared by the author.